Journal of Medicinal Chemistry

Article

pubs.acs.org/jmc

Alternative Chelator for ^{89}Zr Radiopharmaceuticals: Radiolabeling and Evaluation of 3,4,3-(LI-1,2-HOPO)

Melissa A. Deri,[†,‡,§] Shashikanth Ponnala,[†,‡] Brian M. Zeglis,[†] Gabor Pohl,[∥] J. J. Dannenberg,*[,∥] Jason S. Lewis,*[,†] and Lynn C. Francesconi*[,‡,§]

[†]Department of Radiology and the Program in Molecular Pharmacology and Chemistry, Memorial Sloan-Kettering Cancer Center, 1275 York Avenue, New York, New York 10065, United States

[‡]Department of Chemistry, Hunter College of the City University of New York, 695 Park Avenue, New York, New York 10065, United States

[§]Department of Chemistry, The Graduate School of the City University of New York, 365 Fifth Avenue, New York, New York 10016, United States

[∥]Department of Chemistry, City University of New York—Hunter College and the Graduate School, 695 Park Avenue, New York, New York 10065, United States

Supporting Information

ABSTRACT: Zirconium-89 is an effective radionuclide for antibody-based positron emission tomography (PET) imaging because its physical half-life (78.41 h) matches the biological half-life of IgG antibodies. Desferrioxamine (DFO) is currently the preferred chelator for $^{89}Zr^{4+}$; however, accumulation of ^{89}Zr in the bones of mice suggests that $^{89}Zr^{4+}$ is released from DFO in vivo. An improved chelator for $^{89}Zr^{4+}$ could eliminate the release of osteophilic $^{89}Zr^{4+}$ and lead to a safer PET tracer with reduced background radiation dose. Herein, we present an octadentate chelator 3,4,3-(LI-1,2-HOPO) (or HOPO) as a potentially superior alternative to DFO. The HOPO ligand formed a 1:1 Zr-HOPO complex that was evaluated experimentally and theoretically. The stability of ^{89}Zr-HOPO matched or surpassed that of ^{89}Zr-DFO in every experiment. In healthy mice, ^{89}Zr-HOPO cleared the body rapidly with no signs of demetalation. Ultimately, HOPO has the potential to replace DFO as the chelator of choice for ^{89}Zr-based PET imaging agents.

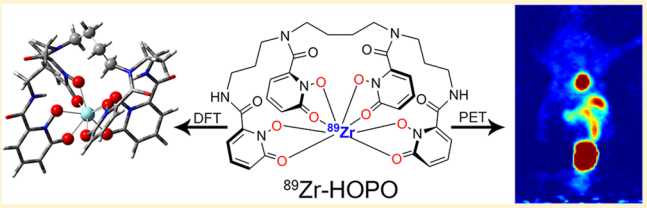

INTRODUCTION

The past few decades have played witness to a revolution in the understanding of the intersection between transition metals and medicine. Not only has the body's management of metals emerged as an important therapeutic target, but metals have become critical components of diagnostic and therapeutic agents. Unsurprisingly, the biomedical importance of chelators (organic molecules capable of binding metals) has increased in parallel to this advent of metals in medicine. The clinical use of chelators is most often associated with treatment for heavy metal poisoning, for example, the administration of ethylenediaminetetraacetic acid (EDTA) to treat lead poisoning.[1,2] However, chelators are also critical components of metal-containing diagnostics and therapeutics, in particular nuclear imaging agents bearing metallic radioisotopes. In these cases, the role of the chelator is to stably sequester the radiometal and prevent its release from the agent. While a number of excellent chelators for common radiometals are known, the recent emergence of a few nontraditional medically useful isotopes have increased the demand for novel chelators specifically tailored to the chemistry of these new radiometals.[3,4] The case of the positron-emitting radiometal zirconium-89 (^{89}Zr) provides a prime example of this phenomenon.

^{89}Zr is readily attracting attention as a radionuclide for positron emission tomography (PET) imaging.[5−12] In the past several years, a wide variety of preclinical studies have been published.[13−19] A number of ^{89}Zr-based imaging agents have been translated into the clinic, including five current clinical trials in the U.S. alone.[20−25] While ^{89}Zr possesses a relatively low energy positron (β_{avg} = 395.5 keV), which affords images with high resolution, the principal driver of its success has been its 78.41 h half-life. A half-life of just over 3 days allows images to be collected multiple days after injection, making it particularly well-suited for the radiolabeling of IgG antibodies. Radioimmunoconjugates have a circulation time of several days, and longer imaging windows allow for both the accumulation of the tracer in the target tissue and the clearance of any unbound tracer from the blood pool. This in turn leads to improved image contrast and tumor-to-background activity ratios.

Yet a radionuclide with suitable decay characteristics is not sufficient to make an effective imaging agent. It is also necessary to have a reliable method of chelating the radiometal and attaching the chelate complex to the targeting vector. In the

Received: March 12, 2014
Published: May 9, 2014

case of ^{89}Zr, the most commonly used chelator is desferrioxamine B (DFO, Figure 1). DFO, a natural bacterial side-

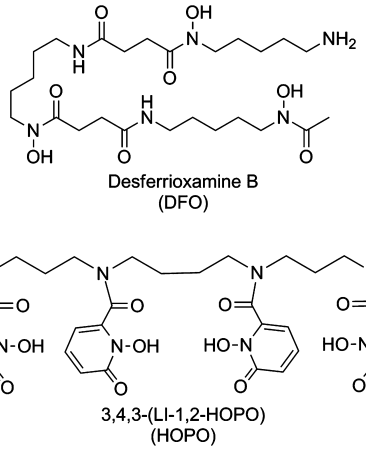

Figure 1. Structures of the currently used chelator for ^{89}Zr, DFO, and the newly investigated alternative chelator, HOPO.

rophore, is a hexadentate ligand with three hydroxamate groups that provide six oxygen donors (three anionic and three neutral) for metal binding.[26] In addition, DFO has a pendent amine that has been derivatized in a number of ways to create bifunctional variants of the chelator for facile conjugation to antibodies and other biomolecular vectors; for example, one such derivative is the commercially available benzyl isothiocyanate DFO.[27] Regardless of which bifunctional DFO derivative is used for conjugation, DFO-mAb conjugates are typically radiolabeled with ^{89}Zr under mild conditions (pH 6.5−8.0, room temp, 1 h).[12,28,29] These radiolabeled bioconjugates can then be purified by either size exclusion chromatography or centrifugal filtration prior to use.

While DFO is currently the gold standard for ^{89}Zr chelation, there is certainly room for improvement. The primary issue with DFO is that even purified ^{89}Zr-DFO-mAb conjugates have been shown to produce significant uptake of radioactivity in the bones of mice, typically on the order of 10 %ID/g.[14,19,30−32] This uptake is not the result of the radioimmunoconjugate as a whole. Rather, the free $^{89}Zr^{4+}$ cation is known to be osteophilic, meaning the metal itself is readily mineralized into the skeleton.[28,33] Therefore, it becomes clear that $^{89}Zr^{4+}$ is being released from its chelator within the body. This uptake of $^{89}Zr^{4+}$ is of particular concern in the clinic, for accumulation of $^{89}Zr^{4+}$ in the bone can dramatically increase radiation dose to the bone marrow, an especially radiosensitive tissue. This concern over in vivo stability has led several groups to investigate the possibility of developing a better chelator for ^{89}Zr.

From an inorganic chemistry perspective, DFO is not ideally suited to the coordination properties of Zr^{4+}. The Zr^{4+} cation is a highly charged, hard Lewis acid with a predilection for forming complexes with high coordination numbers. For example, eight-coordinate complexes such as zirconium oxalate, $[Zr(oxalate)_4]^{4-}$, are particularly common with Zr^{4+}.[34] With this in mind, it seems incongruous that a hexadentate ligand such as DFO is used with a metal that prefers forming octacoordinate complexes. In fact, previous molecular modeling of the most favorable structure of the Zr-DFO complex revealed that in the optimized structure, two water molecules join the metal's coordination sphere to form an eight-coordinate complex.[14] Preliminary work by Brechbiel et al. has focused on investigating the coordination chemistry of Zr^{4+} with different hydroxamate binding groups with the goal of gaining insights toward the design of new chelators.[35] Most notably, this work further confirmed that Zr^{4+} preferentially forms eight-coordinate complexes and thus strengthens the argument for the development of an octadentate chelator.

These data have led us to conclude that a ligand designed specifically with the chemistry of Zr^{4+} in mind may demonstrate improved stability upon complexation with Zr^{4+}. Furthermore and perhaps even more importantly, a more stable complex should be less prone to demetalation in vivo, resulting in reduced bone uptake and thus a safer and more efficient ^{89}Zr-based PET tracer.

Our approach to designing a chelator for Zr^{4+} was inspired by a library of ligands developed by Raymond et al. as actinide sequestration agents.[36] The library contained a number of ligands designed for plutonium(IV) decorporation,[37−39] and the similarity in coordination chemistry between Zr^{4+} and Pu^{4+} marked these as excellent candidates. The use of Hf^{4+} (the third row congener of Zr^{4+}) as a model for Pu^{4+} highlights this connection. These ligands are composed of hard oxygen donor groups, specifically hydroxamates, catecholates, and hydroxypyridinonates.[36] One ligand in particular, 3,4,3-(LI-1,2-HOPO) (Figure 1), stood out as a promising candidate for Zr^{4+} chelation. This ligand, referred to herein as HOPO, is an octadentate chelator composed of a spermine backbone coupled with four hydroxypyridinone groups for metal binding. The hydroxypyridinone groups offer hard, oxygen donors appropriate for binding Zr^{4+} and have pK_a values of −0.8 and 5.8 compared to the much higher pK_a values of the catecholate, hydroxamate, and alkylhydroxamate (pK_a of 9.5, 9.3, and 8.7, respectively).[35,36,40] Zr^{4+} has been shown to successfully compete with Pu^{4+} in extraction experiments using a resin bearing 1,2-hydroxypyridinone groups,[41] which supports our hypothesis that the 1,2-hydroxypyridinone moiety would form a strong chelator for Zr^{4+}. The linear arrangement of donor atoms should impart faster binding kinetics compared to their arrangement in a macrocycle. Taken together, the eight-coordinate binding and the hard oxygen donor groups of the HOPO ligand should be an ideal coordination environment for Zr^{4+} and offer good in vivo stability. While the HOPO ligand is admittedly not novel, its application to $^{89}Zr^{4+}$ and PET is unique.

In this study, we investigate the synthesis and characterization of the HOPO ligand and the Zr-HOPO complex as well as the radiolabeling, characterization, stability, and in vivo behavior of ^{89}Zr-HOPO in comparison to ^{89}Zr-DFO. The comparative stabilities are further investigated by density functional theory (DFT) calculations. Taken together, these studies demonstrate the great potential of 3,4,3-(LI-1,2-HOPO) and that family of ligands as chelators for $^{89}Zr^{4+}$.

RESULTS AND DISCUSSION

An ideal chelator for Zr^{4+} must meet a few core requirements: (1) it must be octadentate to fully saturate the coordination sphere of Zr^{4+}; (2) it must have hard oxygen donors to complement the hard, oxophilic Zr^{4+} cation; (3) it must offer an appropriate sized cavity for the 0.84 Å effective ionic radius of Zr^{4+}.[42] Additionally, an acyclic chelator would be preferred in order to facilitate faster, more efficient radiolabeling conditions. It was with these factors in mind that the HOPO ligand was chosen for investigation as an alternative, more effective chelator for Zr^{4+}.

dx.doi.org/10.1021/jm500389b | J. Med. Chem. 2014, 57, 4849−4860

Synthesis and Characterization. The HOPO ligand was synthesized as previously reported[31,36,43−45] (Scheme S1). However, the adaptation of this ligand for radiochemical applications required additional purification stringency in order to eliminate the possibility of preferentially labeling trace impurities. Therefore, for the investigation at hand, the final product was purified via reverse-phase HPLC.

The high degree of symmetry of HOPO, combined with its flexibility, resulted in a ^{1}H NMR with many overlapping multiplets due to different conformers of the ligand. As a result, the classification of HOPO as one compound with confounding conformers rather than distinct isomers or impurities was based on the identification of the expected compound by mass spectrometry as well as the appearance of a single peak by HPLC analysis (Figures S1 and S2).

The nonradioactive Zr-HOPO complex was formed on the macroscopic scale to facilitate characterization. The complex was formed by mixing the HOPO ligand with a slight excess (1.5 equiv) of $ZrCl_4$ in water at room temperature. The Zr-HOPO product was analyzed by HPLC and eluted as a single peak with a retention time shifted about 30 s compared to the ligand alone (Figure S3). The 1:1 binding of Zr^{4+} and HOPO was confirmed by high resolution mass spectrometry (HRMS), which shows the expected mass signals (859.12, $[M + Na]^+$) (Figure S4). While the ^{1}H NMR of the Zr-HOPO complex contained the same type of complicated overlapping multiplets as the ligand itself, there were significant changes in the signals most closely associated with binding of Zr^{4+} (Figure S5). The participation of the hydroxypyridinone rings in the complexation of zirconium was confirmed through infrared (IR) spectroscopy which shows a red shift in the signals corresponding to the hydroxypyridinone's carbonyl groups (from 1630 to 1610, from 1564 to 1537 cm^{-1}, and from 1375 to 1360 cm^{-1}) as a result of the oxygens binding Zr^{4+} (Figure S6).[46,47] The calculated IR spectra resulting from the DFT work assign these signals to highly coupled asymmetric carbonyl stretches (Figure S7).

Next, the radioactive ^{89}Zr-HOPO complex was synthesized by radiolabeling the HOPO ligand with a neutralized ^{89}Zr solution at a pH of ∼7.0. The identity of the radioactive ^{89}Zr-HOPO species was confirmed through a coelution study wherein both the radioactive and nonradioactive Zr-HOPO complexes were injected into the HPLC system together (Figure 2). Their coelution demonstrates that the ^{89}Zr-HOPO species possesses the same structure and chemistry as the nonradioactive, characterized Zr-HOPO species. HPLC also confirmed the purity of both the HOPO ligand and the Zr-HOPO complex to be higher than 95%. Further characterization of the Zr-HOPO complex was attempted using ultraviolet−visible (UV−vis) spectroscopy; however, the results were inconclusive as the spectral changes associated with the ligand−metal complexation were minimal (Figures S8 and S9).

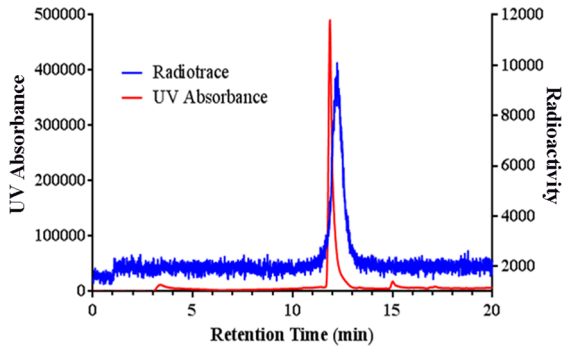

Figure 2. HPLC chromatogram of the co-injection of radioactive ^{89}Zr-HOPO and nonradioactive Zr-HOPO. The ∼30 s separation between the two peaks is due to the sequential setup of the UV and radioactive detectors.

DFT Calculations. The difficulties intrinsic to studying the aqueous chemistry of Zr, and these Zr-ligand complexes in particular, preclude the use of potentiometric titrations or extensive NMR studies because of solubility issues. Therefore, in order to further investigate the coordination chemistry of the Zr-ligand complexes, we performed density functional theory (DFT) calculations on both Zr-HOPO and Zr-DFO. Additionally, the results of the Zr-HOPO calculations led us to investigate a slightly modified HOPO ligand adapted to overcome an observed weakness in the Zr-HOPO structure. DFT calculations were performed using the Gaussian 09[48] suite of computer programs. All calculations used the CEP-121G basis set and the B3LYP functional. We tested four basis sets contained in Gaussian 09 that can treat Zr (CEP-121G, CEP-31G, LanL2DZ, and QZVP), for their accuracy treating the gas phase acidity of two simple alcohols (ethanol and methanol) as a test of their abilities to accurately treat the organic ligands (which are polyalcohols). CEP-121G and QZVP performed the best (and about equally well). We chose CEP-121G, as it used less computational resources. The detailed data can be found in Table S1. The geometries of all the species were completely optimized in all internal degrees of freedom while considering several different conformations of the ligands and complexes. We base our reports on the lowest energy conformations. The vibrational frequencies on the CP-corrected potential energy surface confirmed all structures to be minima (as all frequencies are real) and enabled the calculation of enthalpies at 298 K, using the normal harmonic approximations employed in the Gaussian 09 program.[48] The counterpoise correction for basis set superposition error[49−52] was incorporated via optimization on the CP-corrected potential energy surfaces (CP-OPT)[52] in which two fragments were considered (the Zr and all ligands as a single fragment) for the gas phase calculations. We used these frequencies to calculate the IR spectrum of Zr-HOPO (Figure S7) using a scaling factor of 0.992 which we obtained for the B3LYP/CEP-121G by comparing the C═O stretch of *N*-methylacetamide with the experimental value,[53] as we have done previously for B3LYP/D95**.[54] We used the GaussView[55] program to visualize the spectrum, choosing a resolution of 15 cm^{-1} for the best match to the experimental spectrum.

We used the CPCM polarizable conductor-like solvent continuum model[49,51] with the Bondi[50] (rather than the default UFF[56]) option for the atomic radii used for the cavity as the model for the aqueous bulk. We have recently found that the radii used to define the cavities in CPCM have a significant effect upon the ΔG_{solv} values of both *N*-methylacetamide (NMA) and water.[57] The Bondi radii[50] generally gave the best results when the electrostatic part was used alone, as in this work. We note that CPCM gives ΔG_{solv} values rather than ΔH values. For simplicity, we have labeled as ΔH values the quantities obtained from a normal vibrational correction for enthalpy calculated using the CPCM Hamiltonian. We used single point a posteriori CP corrections for these calculations, as Gaussian 09 does not allow CP-OPT to be used with solvation models.

dx.doi.org/10.1021/jm500389b | J. Med. Chem. 2014, 57, 4849−4860

We calculated the geometry optimized structures of four complexes: (**I**) the Zr-HOPO complex [Zr^{4+} + 3,4,3-(LI-1,2-HOPO)$^{4-}$]; (**II**) a complex of an alternative HOPO-based ligand, where the central aliphatic chain on the backbone possesses three carbons instead of four [Zr^{4+} + 3,3,3-(LI-1,2-HOPO)$^{4-}$]; (**III**) a previously studied Zr-DFO complex [Zr^{4+} + DFO^{2-} + $2H_2O$]$^{2+}$, as well as another conformation of the same complex that we found to be more stable (**IIIa**); and (**IV**) a neutral, uncharged Zr-DFO complex [Zr^{4+} + DFO^{2-} + $2OH^-$] (Figure 3). We considered **III** and **IIIa** for comparison with a previous study on Zr-DFO^{2+} but also included **IV** for a better comparison with **I** and **II**, which are both neutral complexes. All structures were evaluated in the gas phase as well as with the CPCM to mimic an aqueous environment.

The previously reported DFT study[14] of **III** used two different basis sets: LANL2DZ for the Zr and 6-31+G(d) for the DFO and water molecules. Additionally, no correction was made for basis set superposition error (BSSE). We thought it prudent to repeat this calculation using the CEP-121G basis set to provide direct comparison to our calculations. We also further explored the potential energy surface (PES) of **III**, finding a more stable structure, **IIIa**, that contains H-bonds from each of the H atoms on the protonated terminal amine to the oxygens of the DFO (Figure 3). One of the H-bonds is bifurcated (the H interacts with two different oxygens), a common behavior for ammonium salts.[58] We found the ΔH of **IIIa** to be 10.6 kcal/mol lower (gas phase) and 0.9 kcal/mol higher (aqueous solution using CPCM) than **III**. The lower ΔH of **III** in solution is due to the extended terminal ammonium that can be more easily solvated than the internally H-bonded structure of **IIIa**. Table 1 presents the calculated Zr−O bond distances in the five structures detailed above as well as for Zr chelated by four free 1,2-hydoxypyridinone (1,2-HOPO) groups (Figure S10). The bond lengths of an X-ray crystallographic study on a related compound, Zr-(hydroxamate)$_4$, are also included for reference.[9] The Zr−O distances for the DFO oxygens are all longer than those previously reported, but those between Zr and the water oxygens are somewhat shorter (~0.01−0.03 Å, Table 1). However, the orientations of the waters in the two structures are slightly different. The difference might be due to the BSSE correction and/or the loss of basis set balance, especially across the Zr−O bonds. One generally expects bond elongation when optimization is performed on a BSSE-corrected surface, as noted for the Zr−O bonds in Zr-DFO. We have also noted that optimization of certain systems (e.g., water dimer[59]) converge to incorrect structures when small basis sets are used on a surface not corrected for BSSE. Because of the steric problems within the ligand that modification of the Zr-DFO bonds would provoke, changing the orientations of these oxygens would be more difficult than those of the waters.

While Zr-HOPO (**I**) has two more Zr−O interactions than Zr-DFO (**IV**), we could not assume it to be more stable, as **IV** has two Zr−OH interactions to compensate for the missing interactions with the ligand. We used reaction 1 to determine

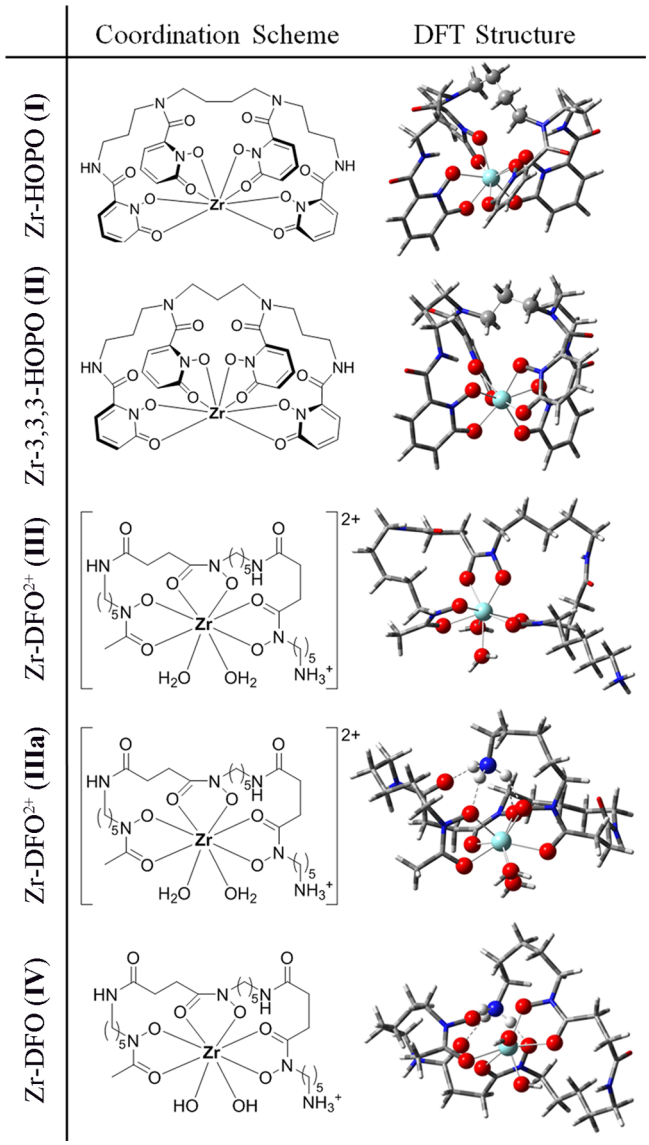

Figure 3. General chemical structures and optimized DFT structures for (**I**) the Zr-HOPO complex; (**II**) a complex of an alternative HOPO-based ligand [3,3,3-(LI-1,2-HOPO)] with Zr; (**III**) a previously studied positively charged Zr-DFO complex; (**IIIa**) a new, more stable conformation of the same charged Zr-DFO complex; and (**IV**) a neutral, uncharged Zr-DFO complex.

Table 1. DFT Calculated Zr−O Bond Lengths[a]

		terminal ligands		central ligands	
I	CO−Zr	2.215	2.158	2.205	2.283
	NO−Zr	2.269	2.326	2.270	2.223
II	CO−Zr	2.220	2.167	2.205	2.291
	NO−Zr	2.266	2.298	2.263	2.218
III (ref 13)	CO−Zr	2.261	2.254	2.199	n/a
	NO−Zr	2.121	2.220	2.111	n/a
III	CO−Zr	2.277	2.284	2.211	n/a
	NO−Zr	2.142	2.249	2.144	n/a
IIIa	CO−Zr	2.262	2.281	2.237	n/a
	NO−Zr	2.197	2.142	2.188	n/a
IV	CO−Zr	2.347	2.362	2.442	n/a
	NO−Zr	2.367	2.229	2.417	n/a
Zr(1,2-HOPO)$_4$	CO−Zr	2.222	2.222	2.212	2.212
	NO−Zr	2.252	2.252	2.242	2.242
Zr(hydroxamate)$_4$ crystal (ref 35)	CO−Zr	2.172	2.196	2.163	2.199
	NO−Zr	2.215	2.233	2.189	2.178

[a]All bond lengths reported in Å. DFT calculations were performed using the Gaussian 09 program with CEP-121G as the basis set.

dx.doi.org/10.1021/jm500389b | J. Med. Chem. 2014, 57, 4849−4860

the relative stability of the two complexes. We note that the structure of $DFOH_2$ has a protonated amine that hydrogen-bonds to three oxygens, one of which is not protonated, which results in a neutral structure (Figure S11).

$$\mathbf{I} + DFOH_2 + 2H_2O \rightarrow \mathbf{IV} + HOPOH_4 \quad (1)$$

The calculated enthalpies of this reaction are 47.9 kcal/mol (gas) and 31.8 kcal/mol (CPCM). These data strongly suggest that Zr-HOPO is more stable than Zr-DFO. The difference between the gas phase and CPCM enthalpies reflects the large solvation free energy of the small OH^- anion. However, the difference seems quite large for two species that each have eight Zr−O interactions. One reason for this large difference appears to be that Zr−O distances found in **IV** are about 0.01 Å larger on average, suggesting these bonds in **IV** to be weaker than in **I** or **II**. These calculations suggest a remarkable improvement in energetic favorability for Zr-HOPO over Zr-DFO.

When we optimized the geometry of **I**, we found several local minima. Structure **I** has the lowest energy, but we thought that we might find a more stable conformation if we eliminated the unfavorable gauche orientation of the $-(CH_2)_4-$ linker between the middle two chelating groups of **I**. As we could not find a more stable structure for **I**, we decided to eliminate one of the CH_2 groups from **I** to form **II**: Zr complexed with a new HOPO-based ligand, 3,3,3-(LI-1,2-HOPO), with a shortened center spacer in the backbone (Figure 3). We expect that the modified ligand of **II** would bind more tightly to the Zr, since it eliminates the unfavorable gauche interaction. To test this hypothesis, we calculated the enthalpy of the reaction that exchanges the ligands of **I** and **II** (reaction 2), which we found to be −2.8 kcal/mol (gas) and −3.2 kcal/mol (CPCM), suggesting that the equilibrium constant for reaction 2 is ∼200 at 298 K.

$$\mathbf{I} + 3,3,3\text{-(LI-1,2-HOPO)} \rightarrow \mathbf{II} + 3,4,3\text{-(LI-1,2-HOPO)} \quad (2)$$

Thus, we expect that **II** would provide even further advantages over **I** as a ligand for Zr^{4+}. Accordingly, we are now exploring this possibility by synthesizing the 3,3,3-(LI-1,2-HOPO) ligand.

Radiolabeling Experiments. Preliminary radiolabeling experiments demonstrated quantitative radiolabeling of 10 mM HOPO with ^{89}Zr within 10 min at room temperature at pH 7 in water. Further experimentation revealed that the time necessary for complete labeling was dependent on ligand concentration, with lower concentrations requiring more time. For example, a HOPO concentration of 10 μM required 45 min to achieve 100% labeling. In general, radiolabeling reactions were left to incubate for 1 h to ensure quantitative labeling, and all radiolabeling reactions were monitored by radioactive thin layer chromatography (radio-TLC).

Radio-TLC analysis of the labeling solutions revealed an interesting concentration-dependent speciation phenomenon (Figure 4). At high concentrations of HOPO (e.g., 10 mM), radio-TLC analysis 10 min after labeling revealed one sharp peak at the origin with a small bump immediately following it. Initially, this seemed like an artifact; however, when radio-TLC analysis is repeated at later time points, this small bump grows into a second, distinct peak. Over time, the first peak slowly converts to the second, and 24 h later, only the second peak remains. These two peaks must represent two different complexes of ^{89}Zr and HOPO, one that is the initial kinetic product and one that is the ultimate thermodynamically stable product. It is significant to note that throughout this conversion

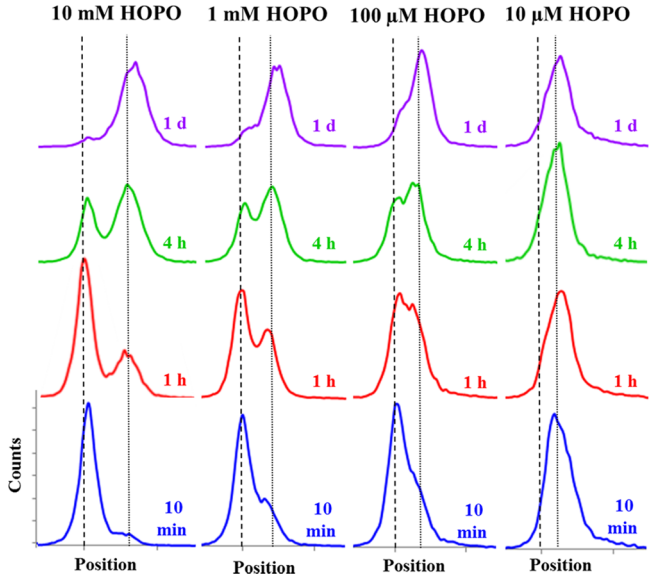

Figure 4. Radio-TLC profiles of the ^{89}Zr-HOPO radiolabeling reaction over time at different concentrations of ligand. Two peaks are observed, with the first peak (the kinetic product) converting to the second peak (the thermodynamic product) over time. The initial area ratio and separation of the two peaks are dependent upon the concentration of the ligand.

(and at every point from 10 min onward) no free $^{89}Zr^{4+}$ is observed. This suggests that all of the $^{89}Zr^{4+}$ is initially complexed by HOPO in some fashion but then over time converts to a different isomer or complex without the $^{89}Zr^{4+}$ ever being released. Most likely, this means the complex undergoes an intramolecular rearrangement of some kind. Upon further investigation, this phenomenon was found to be concentration-dependent. As the concentration of HOPO decreased, two things changed: the secondary peak became increasingly prevalent at early time points, and the two peaks appeared closer together and became less distinguishable by radio-TLC.

The observation that the first peak is less prominent at lower ligand concentrations suggests a possible explanation for the identity of the first peak: a dimer of two ligands simultaneously binding one ^{89}Zr atom. As the concentration of the ligand was decreased, the likelihood of forming such a dimer would also decrease, and thus, the first peak would be less abundant. With this explanation, the second peak is most likely the 1:1 ^{89}Zr-HOPO complex that was expected. This reasoning also explains how the conversion of the first species to the second could take place without releasing the metal. Converting from a dimer to a 1:1 complex seems like a reasonable transformation, as the unused binding groups of one ligand simply replace the binding sites of the second ligand. This hypothesis is supported by the fact that the HPLC coelution study (see above) was carried out 24 h after the initial radiolabeling so that the sample only consisted of the second radio-TLC peak. HPLC analysis showed the compound responsible for the second radio-TLC peak to elute with the characterized 1:1 nonradioactive Zr-HOPO complex, thus confirming its identity.

An explanation for the second observation (that the two peaks get closer together as the ligand concentration decreases) is somewhat more elusive; however, it is a consistently observable trend. The major difficulty in elucidating the exact speciation is that these phenomena seem only to occur at the

dx.doi.org/10.1021/jm500389b | J. Med. Chem. 2014, 57, 4849−4860

Table 2. EDTA Ligand Challenge[a]

Starting Complex	pH	% Intact Starting Species by Incubation Time						
		Initial	1 h	3 h	1 d	3 d	5 d	7 d
^{89}Zr-HOPO	8.0	99.7±0.6	99.8±0.4	100	100	100	100	100
	7.5	100	99.3±1.3	100	100	100	100	100
	7.0	100	99.0±1.8	100	100	100	100	100
	6.5	100	100	100	100	100	100	100
	6.0	100	100	100	100	100	100	99.6±0.7
	5.5	99.5±0.9	100	100	100	100	100	100
	5.0	99.7±0.6	100	100	100	100	100	99.2±1.5
^{89}Zr-DFO	8.0	100	100	100	99.0±0.9	93.0±4.1	87.9±6.7	76.1±11.9
	7.5	100	100	99.3±0.6	97.3±2.3	93.7±3.2	89.9±4.0	75.5±14.1
	7.0	100	100	98.8±0.9	96.7±1.7	95.0±1.8	92.8±3.3	90.4±4.5
	6.5	100	100	98.7±0.8	96.5±1.3	93.4±3.1	90.1±8.5	87.0±6.8
	6.0	100	99.9±0.2	96.2±0.6	93.4±1.8	88.6±5.9	90.0±3.5	80.1±11.6
	5.5	100	97.1±0.8	90.7±1.7	64.7±3.0	44.1±10.0	39.7±12.8	36.3±17.0
	5.0	100	86.6±1.5	55.7±3.8	3.0±0.8	2.4±0.9	1.8±0.4	1.5±0.2

[a]Radiolabeled ligand complexes were incubated with 100-fold excess EDTA at set pH values at 37 °C for 7 days. The experiment was done in triplicate. Green shading indicates >99% intact. Yellow indicates 99−90% intact. Orange indicates 90−80% intact, and red indicates <80% intact.

Table 3. Metal Competition[a]

	% intact starting species by incubation time							
	1 h		1 d		5 d		7 d	
competing metal cation	^{89}Zr-HOPO	^{89}Zr-DFO	^{89}Zr-HOPO	^{89}Zr-DFO	^{89}Zr-HOPO	^{89}Zr-DFO	^{89}Zr-HOPO	^{89}Zr-DFO
Co^{2+}	98.5 ± 2.2	92.5 ± 0.4	98.2 ± 2.6	93.4 ± 3.1	98.6 ± 2.0	96.2 ± 0.5	98.9 ± 1.6	95.8 ± 1.1
Cu^{2+}	98.2 ± 2.5	95.8 ± 4.0	98.1 ± 2.7	98.2 ± 2.6	98.3 ± 2.4	96.8 ± 1.5	98.4 ± 2.3	95.3 ± 0.2
Fe^{3+}	97.0 ± 4.2	90.6 ± 4.5	89.8 ± 5.4	48.2 ± 27.0	90.5 ± 3.8	51.9 ± 11.2	83.0 ± 4.2	39.1 ± 9.9
Ga^{3+}	98.4 ± 2.3	94.2 ± 5.6	97.9 ± 3.0	94.9 ± 4.3	97.3 ± 1.9	93.0 ± 4.4	96.4 ± 0.6	91.1 ± 2.2
Gd^{3+}	98.2 ± 2.6	94.3 ± 1.4	97.8 ± 3.1	95.0 ± 2.7	96.5 ± 2.9	98.4 ± 2.2	94.5 ± 4.1	97.0 ± 0.7
K^{+}	99.0 ± 1.5	97.2 ± 4.0	98.7 ± 1.9	94.8 ± 3.5	98.5 ± 2.2	97.6 ± 0.7	98.1 ± 0.7	97.0 ± 1.6
Mg^{2+}	98.3 ± 2.5	94.4 ± 0.02	98.3 ± 2.5	95.6 ± 2.5	98.6 ± 2.0	98.1 ± 0.8	98.7 ± 1.8	96.5 ± 0.1
Ni^{2+}	98.4 ± 2.3	97.2 ± 4.0	98.4 ± 2.2	94.9 ± 3.2	98.7 ± 1.9	97.0 ± 1.2	97.4 ± 0.1	97.8 ± 1.1
Zn^{2+}	98.6 ± 2.0	92.9 ± 2.2	98.7 ± 1.9	97.9 ± 3.0	97.7 ± 3.3	97.6 ± 3.4	98.3 ± 2.4	96.4 ± 1.3

[a]Radiolabeled ligand complexes were incubated with a 10-fold excess of various biologically relevant metal salts in PBS at a pH of 7.4 at 37 °C for 7 days. The experiment was repeated twice.

tracer level. In these experiments, the ligand concentrations are in the millimolar to micromolar range, while the concentration of ^{89}Zr is in the nanomolar to picomolar range. These conditions cannot be mimicked on the macroscale without inordinate amounts of the HOPO ligand (e.g., ∼3.4 kg of HOPO for every 10 mg of Zr), so analysis is limited to tests that can be carried out on the radioactive samples. Furthermore, as the concentration of the ligand is reduced and approaches that of the metal, the two peaks move closer together to the point where they become indistinguishable. This trend complicates matters because as the two peaks move ever closer together, they begin to appear to be one peak, yet it is impossible to know for certain which of the two original peaks this species represents.

Finally, an alternative explanation for the two peaks is that they simply represent two different coordination structures of the 1:1 Zr-HOPO complex. For example, the initial peak may be HOPO bound to Zr by only six donor groups which converts to the second peak of full octadentate chelation as the final HOPO group changes conformation to bind the metal. While this explanation is consistent with the fact that the conversion between the two species does not involve releasing the metal, it does not provide a justification for the concentration dependence. Further investigations into these speciation phenomena are ongoing.

Stability Studies. *Serum Stability.* In order to gain insight into the in vitro and in vivo kinetic inertness of the Zr-HOPO complex, serum stability tests were performed to simulate biological conditions. Both ^{89}Zr-HOPO and ^{89}Zr-DFO complexes were found to be stable over a 7-day period at 37 °C in human serum (98.8% and 98.3% intact, respectively). Further, no protein-bound ^{89}Zr was observed in the serum samples containing the ^{89}Zr-ligand complexes, which confirms that the complexes remained intact.

EDTA Challenge. Both HOPO and DFO were labeled with ^{89}Zr and then incubated with a 100-fold excess of EDTA at a range of pH values at 37 °C for a period of 7 days in order to examine the stability of the Zr-ligand complexes and their susceptibility to transchelation (Table 2). Analysis of the samples by radio-TLC allowed for the differentiation of the complexes, since ^{89}Zr-EDTA migrates along the ITLC strip, while both ^{89}Zr-DFO and ^{89}Zr-HOPO remain at the origin. DFO was shown to be surprisingly vulnerable to transchelation, most notably at lower pH but also at neutral and biological pH. In contrast, HOPO demonstrated a remarkable resistance to transchelation, remaining >99% intact over the full 7 days for the entire range of pH values tested. The fact that a 100-fold

dx.doi.org/10.1021/jm500389b | J. Med. Chem. 2014, 57, 4849−4860

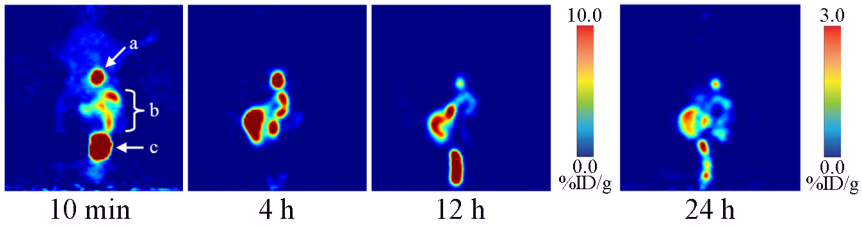

Figure 5. Coronal PET images of ^{89}Zr-HOPO. Healthy mice were administered ^{89}Zr-HOPO (260 μCi [9.6 MBq] in 0.9% sterile saline) via tail vein injection and imaged between 10 min and 24 h after injection. The gall bladder (a), gut (b), and bladder (c) can be visualized. The ^{89}Zr-HOPO complex undergoes rapid renal clearance followed by slower hepatobiliary clearance. No uptake of ^{89}Zr in the bone is observed.

excess of EDTA was unable to strip the ^{89}Zr from HOPO is a testament to the stability of the complex. In contrast, the release of ^{89}Zr from DFO suggests that the ligand is susceptible to transchelation and may experience similar release in vivo to any number of competing substances in the body. Additionally, as tumors are known to be more acidic than healthy tissues, the greatly improved stability of the Zr-HOPO complex over Zr-DFO at lower pH may prove beneficial for cancer imaging.

Metal Cation Competition. As a counterbalance to the EDTA challenge that evaluated the potential for another ligand to outcompete HOPO for the metal cation, a metal competition study was performed to see if other metal cations could outcompete ^{89}Zr for the HOPO binding pocket. Both HOPO and DFO were labeled with ^{89}Zr and then incubated with a 10-fold excess of various metal salts at pH 7.4 at 37 °C (Table 3). The samples were monitored for 7 days by radio-TLC to determine the percentage of intact ^{89}Zr-ligand complex. Both ^{89}Zr-DFO and ^{89}Zr-HOPO proved to be relatively stable (>95% intact) when challenged with the majority of competing metals with the notable exception of Fe^{3+}. In this case, after 7 days of incubation with $FeCl_3$, HOPO released ~17% of the $^{89}Zr^{4+}$ compared with DFO which released >50% of the $^{89}Zr^{4+}$. Since DFO is originally a siderophore, its affinity for iron over zirconium is unsurprising. DFO also exhibited a slight release of $^{89}Zr^{4+}$ in the presence of Ga^{3+} (~9%). This competition further demonstrates the stability of the Zr-HOPO complex and shows an advantage over Zr-DFO.

In Vivo Studies. An advantage of working with a ligand that has already been evaluated for a different biological application is that studies into the toxicity of the compound have already been carried out.[31] The toxicity of HOPO was studied in both mice[43] and baboons,[45] and neither showed any evidence of harm with frequent, repeated injections of the HOPO ligand at concentrations of 10 and 30 μmol/kg, respectively. These data, combined with the fact that the extremely small amounts of compound needed for radiopharmaceutical studies are far below the threshold for pharmacological effects, allowed for the immediate evaluation of ^{89}Zr-HOPO in mice without concerns about adverse reactions.

Imaging. PET imaging studies were performed in order to investigate the in vivo pharmacokinetics of the ^{89}Zr-HOPO complex. To this end, the ^{89}Zr-HOPO complex (260 μCi, 9.6 MBq, in 200 μL of 0.9% sterile saline) was injected into healthy mice and imaged at four time points using PET (Figure 5). At 10 min, the vast majority of the radioactivity is observed in the bladder, which indicates rapid renal clearance. At the remaining time points (4, 12, and 24 h), much of the radioactivity is seen in the gut, signifying hepatobiliary as well as renal excretion. Interestingly, there was significant activity localized in the gall bladder: this is most likely a consequence of the hepatobiliary excretion of the complex through the gut of the mice but is not fully understood at present. This explanation is supported by the fact that the activity in the gall bladder decreases over time. Importantly, no significant bone uptake was observed in the imaging at any time point, indicating that there was no release of the $^{89}Zr^{4+}$ cation from the ligand in vivo. For comparison, previous studies with the ^{89}Zr-DFO complex show only rapid renal clearance of the radiotracer.[14,33,60]

Biodistribution. An ex vivo biodistribution study was also performed in healthy mice to further probe the biological behavior of the ^{89}Zr-HOPO complex The results of this study match the trends observed in the PET images, including the involvement of both the renal and fecal clearance pathways. (Table 4). At 10 min after injection, the activity was found largely in the kidneys (9.46 ± 2.71 %ID/g), suggesting rapid renal excretion, as well as the small intestine (5.99 ± 1.18 %ID/g) and the gall bladder (6.61 ± 2.87 %ID/g), consistent with hepatobiliary excretion. By the 1 h time point, most of the activity had already cleared through the kidneys (1.05 ± 0.51 %ID/g) but was still seen in the gall bladder (6.94 ± 3.38 %ID/g). The large intestine contains the majority of the radioactivity at 4 h (7.17 ± 2.15 %ID/g), while the 12 and 24 h time points demonstrate the further clearance of the remaining activity from all of the organs examined. Notably, the low amount of activity in the bone, which decreases over time (from 1.04 ± 0.44 to 0.17 ± 0.03 %ID/g), is consistent with the clearance of the intact complex rather than accumulation due to mineralization of the free radiometal.

In order to make direct comparisons, the in vivo biodistribution of ^{89}Zr-DFO was investigated in the same study (Figure 6). As expected, ^{89}Zr-DFO cleared exclusively through the kidneys and thus was eliminated more quickly than ^{89}Zr-HOPO. The fact that ^{89}Zr-DFO does not show any gall bladder uptake further suggests that the uptake of ^{89}Zr-HOPO in the gall bladder is a result of hepatobiliary excretion. Other than the difference in excretory pathways, the clearance of the two complexes through the blood and other organs appears similar, with neither complex accumulating appreciably anywhere in the body.

There is a statistically significant difference in the amount of activity in the bone between ^{89}Zr-DFO and ^{89}Zr-HOPO, with higher levels observed for ^{89}Zr-HOPO. This could be the result of the release of the $^{89}Zr^{4+}$ cation from the HOPO ligand due to instability or metabolism; however, if this were the case, we would expect to see a more substantial amount of radioactivity in the bone and for the amount of activity to stay constant or grow over time. Instead, with such a small amount of activity and no evidence of long-term accumulation of the radiometal in the bone, this is most likely a question of the perfusion and clearance kinetics of ^{89}Zr-HOPO rather than demetalation. Since ^{89}Zr-DFO is only cleared renally and not through the

dx.doi.org/10.1021/jm500389b | J. Med. Chem. 2014, 57, 4849−4860

Table 4. Biodistribution Results[a]

	10 min		1 h		4 h		12 h		24 h	
	Zr-HOPO	Zr-DFO	Zr-HOPO	Zr-DFO	Zr-HOPO	Zr-DFO	Zr-HOPO	Zr-DFO	Zr-HOPO	Zr-DFO
blood	3.24 ± 0.66	5.11 ± 0.90	0.17 ± 0.10	0.10 ± 0.04	0.05 ± 0.04	0.03 ± 0.01	0.02 ± 0.00	0.01 ± 0.00	0.02 ± 0.00	0.02 ± 0.02
heart	1.57 ± 0.22	2.17 ± 0.62	0.12 ± 0.06	0.06 ± 0.02	0.06 ± 0.01	0.03 ± 0.01	0.06 ± 0.01	0.02 ± 0.00	0.07 ± 0.01	0.02 ± 0.01
gall bladder	6.61 ± 2.87	1.57 ± 0.25	6.94 ± 3.38	0.47 ± 0.14	1.00 ± 0.41	0.26 ± 0.15	2.45 ± 1.02	0.16 ± 0.14	1.15 ± 0.59	0.23 ± 0.21
liver	3.29 ± 0.75	0.88 ± 0.49	0.22 ± 0.09	0.24 ± 0.07	0.13 ± 0.01	0.12 ± 0.03	0.09 ± 0.02	0.06 ± 0.02	0.06 ± 0.03	0.11 ± 0.02
stomach	1.22 ± 0.39	0.62 ± 0.28	0.30 ± 0.15	1.10 ± 0.51	0.50 ± 0.74	0.06 ± 0.02	0.01 ± 0.00	0.01 ± 0.00	0.02 ± 0.00	0.01 ± 0.01
large intestine	0.26 ± 0.15	0.43 ± 0.13	0.09 ± 0.06	0.02 ± 0.01	7.17 ± 2.15	0.62 ± 0.55	0.10 ± 0.03	0.07 ± 0.05	0.03 ± 0.02	0.02 ± 0.01
small intestine	5.99 ± 1.18	0.94 ± 0.16	1.11 ± 0.35	0.35 ± 0.17	0.12 ± 0.13	0.04 ± 0.02	0.02 ± 0.01	0.01 ± 0.01	0.02 ± 0.00	0.02 ± 0.01
kidney	9.46 ± 2.71	14.44 ± 5.88	1.05 ± 0.51	1.39 ± 0.55	0.40 ± 0.14	1.10 ± 0.44	0.53 ± 0.23	0.36 ± 0.13	0.51 ± 0.29	1.12 ± 0.33
bladder	2.04 ± 1.06	2.50 ± 0.48	0.73 ± 0.36	2.47 ± 1.30	0.58 ± 0.27	1.22 ± 0.77	0.54 ± 0.26	0.69 ± 0.31	0.28 ± 0.14	0.56 ± 0.41
muscle	0.36 ± 0.06	0.73 ± 0.56	0.10 ± 0.03	0.02 ± 0.01	0.09 ± 0.06	0.01 ± 0.01	0.06 ± 0.01	0.01 ± 0.00	0.06 ± 0.01	0.01 ± 0.00
bone	1.04 ± 0.44	0.43 ± 0.10	0.29 ± 0.09	0.07 ± 0.04	0.23 ± 0.12	0.04 ± 0.02	0.25 ± 0.07	0.03 ± 0.01	0.17 ± 0.03	0.06 ± 0.01

[a]All values reported as %ID/g. Healthy, athymic nude mice were injected with either ^{89}Zr-HOPO or ^{89}Zr-DFO (24−35 μCi [0.89−1.29 MBq] in 0.9% sterile saline) via the tail vein, sacrificed at specified time points, and necropsied. Organs were collected, weighed, and measured for radioactivity using a γ counter. $N = 4$ for each compound at each time point.

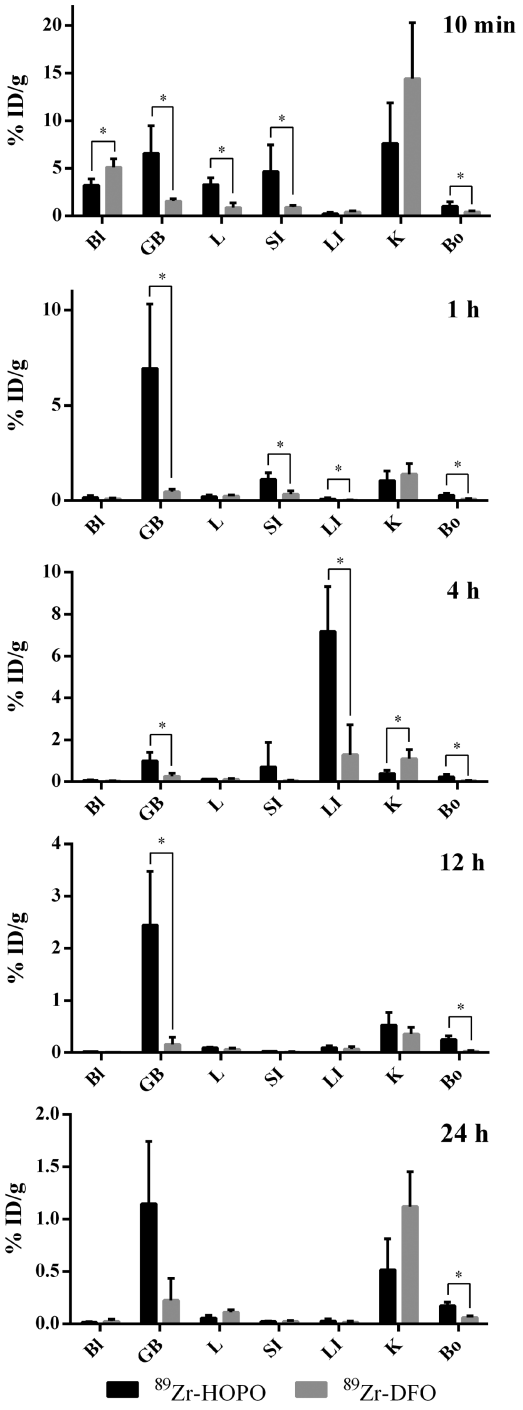

Figure 6. Biodistribution of ^{89}Zr-HOPO and ^{89}Zr-DFO in select organs. Healthy, athymic nude mice were injected with either ^{89}Zr-HOPO or ^{89}Zr-DFO (24−35 μCi [0.89−1.29 MBq] in 0.9% sterile saline) via the tail vein, sacrificed at specified time points, and necropsied. The concentration of radioactivity in the chosen organs is expressed as %ID/g and presented as an average value from four animals ± standard deviation. Bl = blood, GB = gall bladder, L = liver, LI = large intestines, SI = small intestines, K = kidney, Bo = bone. ∗ indicates P values of <0.05.

hepatobiliary system, it is excreted from the body faster than ^{89}Zr-HOPO, as evidenced by the blood clearance curve (Figure 7). We postulate that just as ^{89}Zr-HOPO takes a longer time to clear the blood, it also takes a longer time to clear the bone.

dx.doi.org/10.1021/jm500389b | J. Med. Chem. 2014, 57, 4849−4860

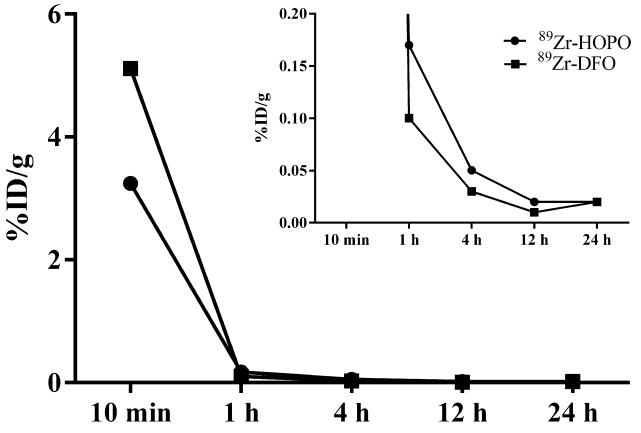

Figure 7. Blood clearance of ^{89}Zr-HOPO and ^{89}Zr-DFO in healthy, athymic nude mice (n = 4) over time. Inset shows a zoomed graph for further detail.

The higher levels of ^{89}Zr measured in the bone are likely a result of higher levels of ^{89}Zr still present in the mouse.

The difference in clearance pathways between ^{89}Zr-HOPO and ^{89}Zr-DFO should not be a concern in the long run. Upon conjugation to an antibody, the pharmacokinetics of the ^{89}Zr-HOPO complex will be completely superseded by those of the biomacromolecule. However, at this point in the development of the ligand, with only the bare ^{89}Zr-ligand complex available, it is only possible to test its in vivo stability for the comparatively short circulation time associated with the small molecule complex as opposed to the several day circulation time of a radioimmunoconjugate. Therefore, while the in vivo stability of the ^{89}Zr-HOPO complex demonstrated here is very promising, it alone is insufficient to prove its viability in ^{89}Zr-HOPO-based radioimmunoconjugates. With this in mind, the longer duration in vitro studies were intended to supplement the in vivo experiments by allowing us to probe the longer stability requirements of the antibody labeling applications. In sum, the combination of the in vitro and in vivo experiments gives a more complete picture of the stability of the ^{89}Zr-HOPO complex and illustrates the great potential of the HOPO ligand.

CONCLUSIONS

In terms of Zr^{4+} chelation and stability, 3,4,3-(LI-1,2-HOPO) has proven to be a superior ligand compared to DFO. We have synthesized the HOPO ligand, synthesized and characterized the Zr-HOPO complex, and evaluated the stability and behavior of the ^{89}Zr-HOPO complex both in vitro and in vivo. HOPO has proven comparable and often superior to DFO in every test we have conducted, both experimentally and computationally. Our DFT calculations have shown Zr^{4+} complexed with HOPO to be significantly more stable than with DFO and have suggested that the complex with 3,3,3-(LI-1,2-HOPO), a modified hydroxypyridinone-based ligand, might be even more stable still. The improved stability of the ^{89}Zr-HOPO complex is most dramatically shown in the EDTA challenge experiments in which the ^{89}Zr-HOPO complex is able to resist transchelation far better than ^{89}Zr-DFO. This increase in stability is especially significant because it is observed not only at lower pHs like 5.0−6.5 at which the lower pK_a of the hydroxypyridinone was an expected advantage but also at biologically relevant pHs like 7.0−7.5 at which DFO was still susceptible to partial transchelation. In addition, we have shown the ^{89}Zr-HOPO complex to have good biological behavior, clearing the body cleanly without any signs of demetalation.

The ultimate test of the efficacy of the HOPO ligand will come when the ligand can be conjugated to an antibody, radiolabeled, and tested in vivo in the context of its desired application. To this end, bifunctionalization of the HOPO ligand is currently underway, and evaluation of the ligand when conjugated to an antibody will be forthcoming once the synthesis is complete. Additionally, the 3,3,3-(LI-1,2-HOPO) ligand is also being synthesized to follow-up on the intriguing results of the DFT calculations which suggest that a shortened backbone will impart even greater stability upon binding of Zr^{4+}. For now, the HOPO ligand shows tremendous promise as a chelator for ^{89}Zr and may eventually supplant DFO for immunoPET applications.

EXPERIMENTAL SECTION

Materials and Methods. All chemicals, unless otherwise noted, were acquired from Sigma-Aldrich (St. Louis, MO) and used as received without further purification. Human serum was purchased frozen from Sigma-Aldrich. All water used was ultrapure (>18.2 MΩ cm^{-1}). All instruments were calibrated and maintained in accordance with standard quality-control procedures. High resolution mass spectrometry (HRMS) measurements were performed on a Waters SYNAPT high definition MS system (ESI-QTOF) and low resolution mass spectra were recorded with a Waters Acquity UPLC with electrospray ionization (ESI) SQ detector. ^{1}H NMR spectra were recorded at ambient temperature on a Bruker 500 MHz NMR with Topsin 2.1 software. The NMR spectra are expressed on the δ scale and were referenced to residual solvent peaks and/or internal tetramethylsilane. The HPLC system used for analysis and purification compounds consisted of a Shimadzu prominence system equipped with a diode array and a radioactive detector (Bioscan Inc., Washington, DC). IR spectroscopy was performed on a solid sample using an attenuated total reflectance attachment on a PerkinElmer Spectrum 2 FT-IR spectrometer with a UATR Two attachment. UV−vis spectroscopy was carried out using a Thermo Scientific Evolution 220 UV−visible spectrophotometer.

^{89}Zr was produced at Memorial Sloan-Kettering Cancer Center on a TR19/9 cyclotron (Ebco Industries Inc.) via the ^{89}Y(p,n)^{89}Zr reaction and purified to yield ^{89}Zr with a specific activity of 196−496 MBq/mg. Activity measurements were made using a CRC-15R dose calibrator (Capintec). For the quantification of activities, experimental samples were counted on an Automatic Wizard (2) g-Counter (PerkinElmer). The radiolabeling of ligands was monitored using salicylic acid impregnated instant thin-layer chromatography paper (ITLC-SA) (Agilent Technologies) and analyzed on a Bioscan AR-2000 radio-TLC plate reader using Winscan Radio-TLC software (Bioscan Inc., Washington, DC). All in vivo experiments were performed according to protocols approved by the Memorial Sloan-Kettering Institutional Animal Care and Use Committee (Protocol 08-07-013). Purity of greater than 95% was confirmed using quantitative HPLC analysis for nonradioactive compounds (HOPO and Zr-HOPO) and radio-TLC for radioactive compounds (^{89}Zr-HOPO).

3,4,3-(LI-1,2-HOPO) (HOPO). The ligand was synthesized as previously described with slight modification. The details are presented in the Supporting Information.

Zr-HOPO. A solution of zirconium chloride (1.5 mg, 6.0 μmol) in water (0.5 mL) was added to a solution of HOPO (3.0 mg, 4.0 μmol) in water (0.5 mL). The mixture was vortexed and left for 15 min. The resulting solution was cloudy with some white precipitate. The complex was not very soluble in water; however, enough compound remained in solution to allow for analysis of the complex via HRMS and HPLC. NMR analysis remained difficult because of low solubility as well as the indistinct, overlapping multiplets of the HOPO ligand itself (Figure S5). A solution of nonradioactive Zr-HOPO was lyophilized, and the resulting off-white powder was analyzed by IR spectroscopy. Characterization of the Zr-HOPO complex by UV−vis

dx.doi.org/10.1021/jm500389b | J. Med. Chem. 2014, 57, 4849−4860

spectroscopy was attempted but not conclusive. The details are presented in the Supporting Information.

Radiolabeling Studies. ^{89}Zr was received after target processing as ^{89}Zr oxalate in 1.0 M oxalic acid. This solution is then neutralized with 1.0 M sodium carbonate to reach pH 6.8−7.2. Both the DFO and HOPO ligands were labeled at various concentrations in water or saline with the neutralized ^{89}Zr solution at room temperature for varying lengths of time, typically 10−60 min. Samples were labeled with 10 μCi to 1 mCi depending on the nature of the experiment (for reference, 1 μCi ^{89}Zr equals 25 fmol). Reactions were monitored via radio-TLC using Varian ITLC-SA strips (Agilent Technologies) and 50 mM EDTA at pH 5 as the mobile phase. ^{89}Zr-ligand complexes remained at the origin, while free ^{89}Zr was taken up by EDTA in the mobile phase and migrated along the ITLC strip.

Serum Stability Study. ^{89}Zr-HOPO and ^{89}Zr-DFO were prepared according to the radiolabeling protocol as described above. For each ^{89}Zr complex, as well as for free, unchelated ^{89}Zr, solutions were made consisting of 1 mL of human serum and 100 μL of the ^{89}Zr species and were placed in a heat block at 37 °C with agitation. Samples were monitored using radio-TLC immediately after mixing and then daily for 1 week. Intact ^{89}Zr-ligand complexes remained at the origin of the ITLC strip, while free ^{89}Zr was either bound by serum proteins or picked up by EDTA in the mobile phase and migrated along the ITLC strip. The stability of the complexes was measured as the percentage of ^{89}Zr that was retained at the origin of the ITLC strip and therefore still bound to the chelator. Free ^{89}Zr incubated in serum appeared on radio-TLC as a series of messy, broad peaks ranging from the origin to the solvent front. This was likely a result of ^{89}Zr being bound to a variety of serum components with different retention factors. In order to confirm that the sharp peaks at the origin seen in the ^{89}Zr-ligand samples were in fact the ^{89}Zr-ligand complexes and not protein-bound ^{89}Zr, size exclusion chromatography (SEC) was performed on the serum samples after 7 days (Figure S12). SEC was carried out with a hand-packed column (18 mm × 180 mm) of Superdex 200 prep grade gel filtration medium (GE Healthcare) on a BioLogic LP automated liquid chromatography system (BioRad) with a flow rate of 1 mL/min for 45 min using PBS as the eluant. Serum protein components were observed in the UV chromatogram (280 nm), while ^{89}Zr species were tracked by γ-counting collected 1 mL fractions. Both ^{89}Zr-ligand serum samples eluted at ∼28 min, which corresponds to the retention time of the pure ^{89}Zr-ligand controls. The control sample of free ^{89}Zr in serum, however, eluted at ∼20 min, which corresponds to the molecular weight of a major serum protein component as seen in the UV chromatogram.

EDTA Challenge Study. The 100 μL samples were prepared consisting of 100 μM ligand to be tested (HOPO or DFO). An amount of 100 μL of ^{89}Zr solution (∼100 μCi) at pH 7 was added to each sample. Each sample was then spotted onto an ITLC strip, developed, and analyzed to obtain an initial measure of the percent labeling. The samples were left to incubate at room temperature for 1 h. Following incubation, 200 μL of 5 mM EDTA at different pH (5.0, 5.5, 6.0, 6.5, 7.0, 7.5, and 8.0) was added to the samples. Lastly, an amount of 100 μL of 500 mM acetate buffer was added to each sample to maintain the experimental pH of the solutions. The final composition of the samples was 500 μL total volume, ∼100 μCi ^{89}Zr, 100 mM acetate buffer, and a 1:100 ratio of ligand/EDTA. The samples were then transferred to a heat block at 37 °C to incubate for 7 days with agitation. Samples were monitored by radio-TLC at 1 h, 3 h, 1 d, 3 d, 5 d, and 7 d postincubation. Three samples were prepared at each pH to obtain triplicate data for statistics.

Metal Cation Competition Study. The 1 mL solutions of 200 μM HOPO and DFO were prepared and radiolabeled with 1 mL (30−50 μCi) of neutralized ^{89}Zr each. Samples were left to incubate at room temperature for 1 h before being monitored by radio-TLC to confirm complete labeling. The ^{89}Zr-ligand samples were then split into 200 μL aliquots and added to 200 μL solutions of prepared 1 mM metal salts [cobalt(II) chloride, copper(II) chloride, iron(III) chloride, gallium(III) nitrate, gadolinium(III) chloride, potassium carbonate, magnesium chloride, nickel(II) acetate, and zinc acetate]. Samples of ^{89}Zr-ligand complexes in competing metal solutions were put in a heat block at 37 °C to incubate with agitation. Sample mixtures were checked by radio-TLC after 1 h, 1 d, 5 d, and 7 d. Experimental data represent the averages and standard deviations of two sets of experiments.

PET Imaging. PET imaging experiments were conducted on a microPET Focus 120. Healthy female, athymic nude mice were administered ^{89}Zr-HOPO (9.6 MBq [260 μCi] in 200 μL of 0.9% sterile saline) via intravenous tail vein injection (t = 0). Approximately 5 min prior to the acquisition of PET images, mice were anesthetized by inhalation of 2% isoflurane (Baxter Healthcare, Deerfield, IL)/oxygen gas mixture and placed on the scanner bed; anesthesia was maintained using 1% isoflurane/gas mixture. PET data for each mouse were recorded via static scans at various time points between 10 min and 24 h. An energy window of 350−700 keV and a coincidence timing window of 6 ns were used. Data were sorted into 2D histograms by Fourier rebinning, and transverse images were reconstructed by filtered back-projection (FBP) into a 128 × 128 × 63 (0.72 × 0.72 × 1.3 mm^3) matrix. The image data were normalized to correct for nonuniformity of response of the PET, dead-time count losses, positron branching ratio, and physical decay to the time of injection, but no attenuation, scatter, or partial-volume averaging correction was applied. The counting rates in the reconstructed images were converted to activity concentrations (percentage injected dose per gram of tissue, %ID/g) by use of a system calibration factor derived from the imaging of a mouse-sized water-equivalent phantom containing ^{89}Zr. Images were analyzed using ASIPro VM software (Concorde Microsystems).

Biodistribution. Acute in vivo biodistribution studies were performed in order to evaluate the uptake of the ^{89}Zr-HOPO and ^{89}Zr-DFO in healthy female, athymic nude mice. Mice were warmed gently with a heat lamp for 5 min before administration of ^{89}Zr-HOPO (0.89−1.11 MBq [24−30 μCi] in 200 μL of 0.9% sterile saline) or ^{89}Zr-DFO (1.11−1.29 MBq [30−35 μCi] in 200 μL of 0.9% sterile saline) via intravenous tail vein injection (t = 0). Animals (n = 4 per group) were euthanized by CO_2(g) asphyxiation at 10 min, 1 h, 4 h, 12 h, and 24 h. After asphyxiation, 14 organs were removed, rinsed in water, dried in air for 5 min, weighed, and counted in a γ counter calibrated for ^{89}Zr. Counts were converted into activity using a calibration curve generated from known standards. Count data were background- and decay-corrected to the time of injection, and the percent injected dose per gram (%ID/g) for each tissue sample was calculated by normalization to the total activity injected. The full data set of organs is included in the Supporting Information (Table S2) along with values represented in %ID without normalization (Table S3). Biodistribution data were assessed by unpaired t tests using GraphPad Prism (version 6.02 for Windows GraphPad Software, San Diego, CA, U.S.) in order to determine any significant differences (p < 0.05) (Table S4).

■ ASSOCIATED CONTENT

Ⓢ Supporting Information

Detailed data and figures from ligand and complex characterization, DFT calculations, serum stability studies, mouse imaging, and biodistribution studies. This material is available free of charge via the Internet at http://pubs.acs.org.

■ AUTHOR INFORMATION

Corresponding Authors

*J.J.D.: phone, 212-772-5343; e-mail, jdannenberg@gc.cuny.edu.

*J.S.L.: phone, 646-888-3038; e-mail, lewisj2@mskcc.org.

*L.C.F.: phone, 212-772-5353; e-mail, lfrances@hunter.cuny.edu.

Author Contributions

All authors have given approval to the final version of the manuscript.

Notes

The authors declare no competing financial interest.

■ ACKNOWLEDGMENTS

The authors thank Blesida Punzalan and Kuntal Sevak for skillful tail-vein injections, Amandeep Saini for assistance in carrying out radio-TLC experiments, Dr. Ben Burton-Pye for spectroscopic advice, and Dr. Xinxu Shi, Dr. David Mootoo, Ahmad Altiti, and Dr. Malleswari Ponnala for early synthetic assistance. The authors are grateful to Professor Ken Czerwinski for helpful discussions. Services provided by the MSKCC Small-Animal Imaging Core Facility were supported in part by NIH Grants R24 CA83084 and P30 CA08748. We gratefully acknowledge the CTSC grant UL1TR000457 of the National Center for Advancing Translational Sciences of the National Institutes of Health. The authors also thank the NIH (Award 1F31CA180360-01, M.A.D.), the NSF (Award IGERT 0965983, L.C.F.), the DOD (Award CDMRP W81XWH-12-1-0029, B.M.Z.), and the DOE (Award FG02-09ER16097, L.C.F., and Award DE-SC0002184, J.S.L.) for their generous funding. Research infrastructure at Hunter College is partially supported by Grant Number MD007599 from the National Institute on Minority Health and Health Disparities (NIMHD) of the NIH.

■ ABBREVIATIONS USED

DFO, desferrioxamine B; HOPO, 3,4,3-(LI-1,2-HOPO); radio-TLC, radioactive thin layer chromatography; SEC, size exclusion chromatography

■ REFERENCES

(1) Sinicropi, M.; Amantea, D.; Caruso, A.; Saturnino, C. Chemical and Biological Properties of Toxic Metals and Use of Chelating Agents for the Pharmacological Treatment of Metal Poisoning. *Arch. Toxicol.* **2010**, *84*, 501−520.

(2) Baran, E. J. Chelation Therapies: A Chemical and Biochemical Perspective. *Curr. Med. Chem.* **2010**, *17*, 3658−3672.

(3) Price, E. W.; Orvig, C. Matching Chelators to Radiometals for Radiopharmaceuticals. *Chem. Soc. Rev.* **2014**, *43*, 260−290.

(4) Zeglis, B. M.; Houghton, J. L.; Evans, M. J.; Viola-Villegas, N.; Lewis, J. S. Underscoring the Influence of Inorganic Chemistry on Nuclear Imaging with Radiometals. *Inorg. Chem.* **2013**, *53*, 1880−1899.

(5) Deri, M. A.; Zeglis, B. M.; Francesconi, L. C.; Lewis, J. S. PET Imaging with ^{89}Zr: From Radiochemistry to the Clinic. *Nucl. Med. Biol.* **2013**, *40*, 3−14.

(6) Vugts, D. J.; van Dongen, G. A. M. S. ^{89}Zr-Labeled Compounds for PET Imaging Guided Personalized Therapy. *Drug Discovery Today: Technol.* **2011**, *8*, e53−e61.

(7) Severin, G. W.; Engle, J. W.; Barnhart, T. E.; Nickles, R. J. Zr-89 Radiochemistry for Positron Emission Tomography. *Med. Chem.* **2012**, *7*, 389−394.

(8) Hohn, A.; Zimmermann, K.; Schaub, E.; Hirzel, W.; Schubiger, P. A.; Schibli, R. Production and Separation of "Non-Standard" PET Nuclides at a Large Cyclotron Facility: The Experiences at the Paul Scherrer Institute in Switzerland. *Q. J. Nucl. Med. Mol. Imaging* **2008**, *52*, 145−150.

(9) Zhang, Y.; Hong, H.; Cai, W. PET Tracers Based on Zirconium-89. *Curr. Radiopharm.* **2011**, *4*, 131−9.

(10) Rice, S. L.; Roney, C. A.; Daumar, P.; Lewis, J. S. The Next Generation of Positron Emission Tomography Radiopharmaceuticals in Oncology. *Semin. Nucl. Med.* **2011**, *41*, 265−282.

(11) Ikotun, O. F.; Lapi, S. E. The Rise of Metal Radionuclides in Medical Imaging: Copper-64, Zirconium-89 and Yttrium-86. *Future Med. Chem.* **2011**, *3*, 599−621.

(12) Zeglis, B. M.; Lewis, J. S. A Practical Guide to the Construction of Radiometallated Bioconjugates for Positron Emission Tomography. *Dalton Trans.* **2011**, *40*, 6168−6195.

(13) Ulmert, D.; Evans, M. J.; Holland, J. P.; Rice, S. L.; Wongvipat, J.; Pettersson, K.; Abrahamsson, P.-A.; Scardino, P. T.; Larson, S. M.; Lilja, H.; Lewis, J. S.; Sawyers, C. L. Imaging Androgen Receptor Signaling with a Radiotracer Targeting Free Prostate-Specific Antigen. *Cancer Discovery* **2012**, *2*, 320−327.

(14) Holland, J. P.; Divilov, V.; Bander, N. H.; Smith-Jones, P. M.; Larson, S. M.; Lewis, J. S. Zr-89-DFO-J591 for ImmunoPET of Prostate-Specific Membrane Antigen Expression in Vivo. *J. Nucl. Med.* **2010**, *51*, 1293−1300.

(15) Munnink, T. H. O.; Arjaans, M. E. A.; Timmer-Bosscha, H.; Schroder, C. P.; Hesselink, J. W.; Vedelaar, S. R.; Walenkamp, A. M. E.; Reiss, M.; Gregory, R. C.; Lub-de Hooge, M. N.; de Vries, E. G. E. PET with the Zr-89-Labeled Transforming Growth Factor-Beta Antibody Fresolimumab in Tumor Models. *J. Nucl. Med.* **2011**, *52*, 2001−2008.

(16) Nagengast, W. B.; de Korte, M. A.; Munnink, T. H. O.; Timmer-Bosscha, H.; den Dunnen, W. F.; Hollema, H.; de Jong, J. R.; Jensen, M. R.; Quadt, C.; Garcia-Echeverria, C.; van Dongen, G. A. M. S.; Lub-de Hooge, M. N.; Schroder, C. P.; de Vries, E. G. E. (89)Zr-Bevacizumab PET of Early Antiangiogenic Tumor Response to Treatment with Hsp90 Inhibitor NVP-AUY922. *J. Nucl. Med.* **2010**, *51*, 761−767.

(17) Perk, L. R.; Walsum, M. S.-v.; Visser, G. W. M.; Kloet, R. W.; Vosjan, M. J. W. D.; Leemans, C. R.; Giaccone, G.; Albano, R.; Comoglio, P. M.; van Dongen, G. A. M. S. Quantitative PET Imaging of Met-Expressing Human Cancer Xenografts with Zr-89-Labelled Monoclonal Antibody DN30. *Eur. J. Nucl. Med. Mol. Imaging* **2008**, *35*, 1857−1867.

(18) Verel, I.; Visser, G. W. M.; Boellaard, R.; Boerman, O. C.; van Eerd, J.; Snow, G. B.; Lammertsma, A. A.; van Dongen, G. Quantitative Zr-89 Immuno-PET for in Vivo Scouting of Y-90-Labeled Monoclonal Antibodies in Xenograft-Bearing Nude Mice. *J. Nucl. Med.* **2003**, *44*, 1663−1670.

(19) Viola-Villegas, N. T.; Rice, S. L.; Carlin, S.; Wu, X.; Evans, M. J.; Sevak, K. K.; Drobjnak, M.; Ragupathi, G.; Sawada, R.; Scholz, W. W.; Livingston, P. O.; Lewis, J. S. Applying PET to Broaden the Diagnostic Utility of the Clinically Validated CA19.9 Serum Biomarker for Oncology. *J. Nucl. Med.* **2013**, *54*, 1876−1882.

(20) Perk, L. R.; Visser, O. J.; Walsum, M. S.-v.; Vosjan, M. J. W. D.; Visser, G. W. M.; Zijlstra, J. M.; Huijgens, P. C.; van Dongen, G. A. M. S. Preparation and Evaluation of Zr-89-Zevalin for Monitoring of Y-90-Zevalin Biodistribution with Positron Emission Tomography. *Eur. J. Nucl. Med. Mol. Imaging* **2006**, *33*, 1337−1345.

(21) Borjesson, P. K. E.; Jauw, Y. W. S.; Boellaard, R.; de Bree, R.; Comans, E. F. I.; Roos, J. C.; Castelijns, J. A.; Vosjan, M.; Kummer, J. A.; Leemans, C. R.; Lammertsma, A. A.; van Dongen, G. Performance of Immuno-Positron Emission Tomography with Zirconium-89-Labeled Chimeric Monoclonal Antibody U36 in the Detection of Lymph Node Metastases in Head and Neck Cancer Patients. *Clin. Cancer Res.* **2006**, *12*, 2133−2140.

(22) Dijkers, E. C. F.; Kosterink, J. G. W.; Rademaker, A. P.; Perk, L. R.; van Dongen, G. A. M. S.; Bart, J.; de Jong, J. R.; de Vries, E. G. E.; Lub-de Hooge, M. N. Development and Characterization of Clinical-Grade Zr-89-Trastuzumab for Her2/Neu ImmunoPET Imaging. *J. Nucl. Med.* **2009**, *50*, 974−981.

(23) Boerjesson, P. K. E.; Jauw, Y. W. S.; de Bree, R.; Roos, J. C.; Castelijns, J. A.; Leemans, C. R.; van Dongen, G. A. M. S.; Boellaard, R. Radiation Dosimetry of Zr-89-Labeled Chimeric Monoclonal Antibody U36 As Used for Immuno-PET in Head and Neck Cancer Patients. *J. Nucl. Med.* **2009**, *50*, 1828−1836.

(24) Dijkers, E. C.; Munnink, T. H. O.; Kosterink, J. G.; Brouwers, A. H.; Jager, P. L.; de Jong, J. R.; van Dongen, G. A.; Schroder, C. P.; Lub-de Hooge, M. N.; de Vries, E. G. Biodistribution of Zr-89-Trastuzumab and PET Imaging of Her2-Positive Lesions in Patients with Metastatic Breast Cancer. *Clin. Pharmacol. Ther.* **2010**, *87*, 586−592.

(25) http://clinicaltrials.gov/ct2/results?term=89Zr&cntry1=NA%3AUS (accessed October 28 2013).
(26) Meijs, W. E.; Herscheid, J. D. M.; Haisma, H. J.; Pinedo, H. M. Evaluation of Desferal as a Bifunctional Chelating Agent for Labeling Antibodies with Zr-89. *Appl. Radiat. Isot.* **1992**, *43*, 1443−1447.
(27) Perk, L. R.; Vosjan, M. J. W. D.; Visser, G. W. M.; Budde, M.; Jurek, P.; Kiefer, G. E.; van Dongen, G. A. M. S. *p*-Isothiocyanatobenzyl-Desferrioxamine: A New Bifunctional Chelate for Facile Radiolabeling of Monoclonal Antibodies with Zirconium-89 for Immuno-PET Imaging. *Eur. J. Nucl. Med. Mol. Imaging* **2010**, *37*, 250−259.
(28) Meijs, W. E.; Haisma, H. J.; Klok, R. P.; vanGog, F. B.; Kievit, E.; Pinedo, H. M.; Herscheid, J. D. M. Zirconium-Labeled Monoclonal Antibodies and Their Distribution in Tumor-Bearing Nude Mice. *J. Nucl. Med.* **1997**, *38*, 112−118.
(29) Holland, J. P.; Sheh, Y.; Lewis, J. S. Standardized Methods for the Production of High Specific-Activity Zirconium-89. *Nucl. Med. Biol.* **2009**, *36*, 729−739.
(30) Munnink, T. H. O.; de Korte, M. A.; Nagengast, W. B.; Timmer-Bosscha, H.; Schroder, C. P.; de Jong, J. R.; van Dongen, G. A. M. S.; Jensen, M. R.; Quadt, C.; Lub-de Hooge, M. N.; de Vries, E. G. E. Zr-89-Trastuzumab PET Visualises Her2 Downregulation by the Hsp90 Inhibitor NVP-AUY922 in a Human Tumour Xenograft. *Eur. J. Cancer* **2010**, *46*, 678−684.
(31) Xu, J.; Durbin, P. W.; Kullgren, B.; Ebbe, S. N.; Uhlir, L. C.; Raymond, K. N. Synthesis and Initial Evaluation for In Vivo Chelation of Pu(IV) of a Mixed Octadentate Spermine-Based Ligand Containing 4-Carbamoyl-3-hydroxy-1-methyl-2(1*H*)-pyridinone and 6-Carbamoyl-1-hydroxy-2(1*H*)-pyridinone. *J. Med. Chem.* **2002**, *45*, 3963−3971.
(32) Nayak, T. K.; Garmestani, K.; Milenic, D. E.; Brechbiel, M. W. PET and MRI of Metastatic Peritoneal and Pulmonary Colorectal Cancer in Mice with Human Epidermal Growth Factor Receptor 1-Targeted Zr-89-Labeled Panitumumab. *J. Nucl. Med.* **2012**, *53*, 113−120.
(33) Abou, D. S.; Ku, T.; Smith-Jones, P. M. In Vivo Biodistribution and Accumulation of ^{89}Zr in Mice. *Nucl. Med. Biol.* **2011**, *38*, 675−81.
(34) Durbin, P. W.; Kullgren, B.; Xu, J.; Raymond, K. N. Development of Decorporation Agents for the Actinides. *Radiat. Prot. Dosim.* **1998**, *79*, 433−443.
(35) Guerard, F.; Lee, Y.-S.; Tripier, R.; Szajek, L. P.; Deschamps, J. R.; Brechbiel, M. W. Investigation of Zr(IV) and ^{89}Zr(IV) Complexation with Hydroxamates: Progress towards Designing a Better Chelator Than Desferrioxamine B for Immuno-PET Imaging. *Chem. Commun.* **2013**, *49*, 1002−1004.
(36) Gorden, A. E. V.; Xu, J.; Raymond, K. N.; Durbin, P. Rational Design of Sequestering Agents for Plutonium and Other Actinides. *Chem. Rev.* **2003**, *103*, 4207−4282.
(37) Hoard, J. L.; Silverton, J. V. Stereochemistry of Discrete Eight-Coordination. I. Basic Analysis. *Inorg. Chem.* **1963**, *2*, 235−242.
(38) Burgada, R.; Bailly, T.; Noël, J. P.; Gomis, J. M.; Valleix, A.; Ansoborlo, E.; Hengé-Napoli, M. H.; Paquet, F.; Gourmelon, P. Synthesis of 3,4,3 LI 1,2 HOPO Labelled with ^{14}C. *J. Labelled Compd. Radiopharm.* **2001**, *44*, 13−19.
(39) Chang, A. J.; De Silva, R. A.; Lapi, S. E. Development and Characterization of ^{89}Zr-Labeled Panitumumab for Immuno-Positron Emission Tomographic Imaging of the Epidermal Growth Factor Receptor. *Mol. Imaging* **2013**, *12*, 17−27.
(40) Glen, G. L.; Silverton, J. V.; Hoard, J. L. Stereochemistry of Discrete Eight-Coordination. III. Tetrasodium Tetrakisoxalatozirconate(IV) Trihydrate. *Inorg. Chem.* **1963**, *2*, 250−255.
(41) Deblonde, G. J. P.; Sturzbecher-Hoehne, M.; Abergel, R. J. Solution Thermodynamic Stability of Complexes Formed with the Octadentate Hydroxypyridinonate Ligand 3,4,3-LI(1,2-HOPO): A Critical Feature for Efficient Chelation of Lanthanide(IV) and Actinide(IV) Ions. *Inorg. Chem.* **2013**, *52*, 8805−8811.
(42) Shannon, R. D. Revised Effective Ionic Radii and Systematic Studies of Interatomic Distances in Halides and Chalcogenides. *Acta Crystallogr. A* **1976**, *32*, 751−767.
(43) Durbin, P. W.; Kullgren, B.; Raymond, K. N. Multidentate Hydroxypyridinonate Ligands for Pu(IV) Chelation in Vivo: Comparative Efficacy and Toxicity in Mouse of Ligands Containing 1,2-HOPO or Me-3,2-HOPO. *Int. J. Radiat. Biol.* **2000**, *76*, 199−214.
(44) Bailly, T.; Burgada, R. Nouvelle Méthode De Synthèse Du 3,4,3 LI 1,2 HOPO (1,5,10,14-Tétra (1-hydroxy-2-pyridone-6 oyl) 1,5,10,14 tétraazatétradécane). *C. R. Acad. Sci., Ser. IIC* **1998**, *1*, 241−245.
(45) Fritsch, P.; Herbreteau, D.; Moutairou, K.; Lantenois, G.; Richard-le Naour, H.; Grillon, G.; Hoffschir, D.; Poncy, J. L.; Laurent, A.; Masse, R. Comparative Toxicity of 3,4,3-LIHOPO and DTPA in Baboons: Preliminary Results. *Radiat. Prot. Dosim.* **1994**, *53*, 315−318.
(46) Simanova, A. Molecular Perspectives on Goethite Dissolution in the Presence of Oxalate and Desferrioxamine-B. Umeå University: Umeå, Sweden, 2011.
(47) Yang, J.; Bremer, P. J.; Lamont, I. L.; McQuillan, A. J. Infrared Spectroscopic Studies of Siderophore-Related Hydroxamic Acid Ligands Adsorbed on Titanium Dioxide. *Langmuir* **2006**, *22*, 10109−10117.
(48) Frisch, M. J.; Trucks, G. W.; Schlegel, H. B.; Scuseria, G. E.; Robb, M. A.; Cheeseman, J. R.; Scalmani, G.; Barone, V.; Mennucci, B.; Petersson, G. A.; et al. *Gaussian 09*, revision A.2; Gaussian, Inc.: Wallingford, CT, 2009.
(49) Barone, V.; Cossi, M. Quantum Calculation of Molecular Energies and Energy Gradients in Solution by a Conductor Solvent Model. *J. Phys. Chem. A* **1998**, *102*, 1995−2001.
(50) Bondi, A. van der Waals Volumes and Radii. *J. Phys. Chem.* **1964**, *68*, 441−451.
(51) Cossi, M.; Rega, N.; Scalmani, G.; Barone, V. Energies, Structures, and Electronic Properties of Molecules in Solution with the C-PCM Solvation Model. *J. Comput. Chem.* **2003**, *24*, 669−681.
(52) Simon, S.; Duran, M.; Dannenberg, J. J. How Does Basis Set Superposition Error Change the Potential Surfaces for Hydrogen-Bonded Dimers? *J. Chem. Phys.* **1996**, *105*, 11024−11031.
(53) Watson, T. M.; Hirst, J. D. Calculating Vibrational Frequencies of Amides: From Formamide to Concanavalin A. *Phys. Chem. Chem. Phys.* **2004**, *6*, 998−1005.
(54) Viswanathan, R.; Dannenberg, J. J. A Density Functional Theory Study of Vibrational Coupling in the Amide I Band of B-Sheet Models. *J. Phys. Chem. B* **2008**, *112*, 5199−5208.
(55) Dennington, R.; Keith, T.; Millam, J. *GaussView*, version 5; Semichem Inc.: Shawnee Mission, KS, 2009.
(56) Rappe, A. K.; Casewit, C. J.; Colwell, K. S.; Goddard, W. A.; Skiff, W. M. Uff, a Full Periodic Table Force Field for Molecular Mechanics and Molecular Dynamics Simulations. *J. Am. Chem. Soc.* **1992**, *114*, 10024−10035.
(57) Marianski, M.; Dannenberg, J. J. Unpublished results.
(58) Jeffrey, G. A., Saenger, W., Eds. *Hydrogen Bonding in Biological Structures*; Springer-Verlag: Berlin, 1991; pp 136−43.
(59) Plumley, J. A.; Dannenberg, J. J. A Comparison of the Behavior of Functional/Basis Set Combinations for Hydrogen-Bonding in the Water Dimer with Emphasis on Basis Set Superposition Error. *J. Comput. Chem.* **2011**, *32*, 1519−1527.
(60) Meijs, W. E.; Haisma, H. J.; VanderSchors, R.; Wijbrandts, R.; VandenOever, K.; Klok, R. P.; Pinedo, H. M.; Herscheid, J. D. M. A Facile Method for the Labeling of Proteins with Zirconium Isotopes. *Nucl. Med. Biol.* **1996**, *23*, 439−448.